THE INVESTIGATION OF NON-BUOYANT SMOKE RINGS

A Thesis

Presented to

the Faculty of the Department of Civil Engineering

University of Houston

In Partial Fulfillment

of the Requirements for the Degree

Master of Science in Civil Engineering

---

by

Tae Hoon Yoon

June, 1967

ACKNOWLEDGEMENTS

The writer wishes to express his deepest gratitude to Dr. N. H. C. Hwang for serving as Chairman of the Committee and for his encouraging guidance towards the completion of this thesis.

Sincere appreciation is due Dr. R. Blumberg and Dr. C. Dalton for serving on the Committee, especially for Dr. Dalton's many suggestions throughout the writing of this thesis.

The financial support of the National Science Foundation Grant GK-306 to enable the project is gratefully acknowledged.

THE INVESTIGATION OF NON-BUOYANT SMOKE RINGS

An Abstract of a Thesis

Presented to

the Faculty of the Department of Civil Engineering

University of Houston

In Partial Fulfillment

of the Requirements for the Degree

Master of Science in Civil Engineering

---

by

Tae Hoon Yoon

June, 1967

ABSTRACT

General characteristics of the isolated masses of a non-buoyant fluid puff released in a fluid of identical density have been investigated. However, this is not the case with the horizontal motion of a compressible fluid. This study is so conducted as to probe the phenomena of motion of the smoke ring which moves through and associates with its confined and unstratified surroundings.

The Eulerian velocities of the ring along the ring axis, the momentum, and the numerical constants related to the ring motion are studied in this dissertation both analytically and experimentally. The results are presented as functions of elapsed time or distance corresponding to the time. Two distinguished regions of ring motion have been found experimentally by the sudden change of characteristic dimension of the ring as it travels downstream. It is observed that the Eulerian velocities, momentum, and force acting on the ring in each region are distinguishably different. They may be approximately predicted by the theories of ideal fluids in the first (or initial) region, and by theories of turbulent flow in the second (or "turbulent") region.

TABLE OF CONTENTS

LIST OF PLATES

LIST OF FIGURES

NOMENCLATURE

A	Cross-sectional area of ring in the advance direction of the ring
a	Radius of cross section of isolated vortex filament
C	Numerical constant
D	diameter of outlet
F	Force acting on ring
L,M,N	Arbitrary function
I	Momentum
m	Mass of fluid
n	Numerical constant
n_1	Numerical constant
P	Impulse
r	Radius of ring
r_0	Radius of outlet
R_0	Non-dimensional radius of outlet, r_0/D
r,θ,x	Cylindrical coordinates
R,X	Non-dimensional cylindrical coordinates (r/D,x/D)
t_0	Time interval between the origin of coordinates and actual starting point of ring motion (virtual origin)
t	Time
T	Energy
U	Mean velocity in x-direction
U_0	Mean velocity along ring-axis

U_5	Velocity U_0 at $X = 5$
u	Velocity component in x-direction
v	Velocity component in y-direction and r-direction
w	Velocity component in z-direction
Q	Volume rate
V	Velocity of advance of ring
V_0	Velocity V along ring-axis
V_{20}	Velocity V_0 at $X = 20$
Γ	Circulation
ρ	Density of fluid
s, β	Cylindrical coordinate in the cross section of vortex filament
ϕ	Distance from the coordinates of a vortex filament to a point in fluid
Ψ	Stream function
ξ	Vorticity component in y-z plane
η	Vorticity component in x-z plane
ζ	Vorticity component in x-y plane and r-x plane

CHAPTER I

INTRODUCTION

In 1952, Bowen [1] observed that in certain demolition explosions, smoke rings were formed which maintained their shape to considerable heights. He first investigated this phenomenon in the interest that it may be possible to use such rings in rain-making experiments to project seeding material into clouds. Bowen's observations showed the initial cloud formed by explosion was approximately symmetrical, and rose rapidly from the flat ground. In about 10 to 15 seconds it had clearly formed a smoke ring. As it rose higher, the diameter of the ring increased and the cross-sectional area of the vortex filament decreased; this process continued until the ring broke up about 10 minutes later at about 5,000 ft., at which elevation there was later found to be an inversion.

Laboratory experiments on buoyant rings and other related puff motions have been studied by Turner [2], Grigg and Stewart [3], and Richards [4]. Their works indicate that there is a fundamental difference in behavior of vortex rings projected upwards, according to whether they do or do not contain fluid which is lighter than the surroundings.

This study is designed to investigate the motion of a non-buoyant vortex ring with finite initial momentum at an outlet and which travels horizontally through unstratified surroundings in which the effect of body forces is neglected.

CHAPTER II

THEORETICAL REVIEW OF THE PROBLEM

I. DERIVATION OF THE MOTION OF THE RING IN ITS INITIAL STAGE

When a circular vortex ring is first puffed out, the motion may be assumed to be laminar. Spreading of the vorticity from the core is caused mainly by a molecular diffusion, the effect of which is rather insignificant compared with the main motion. It is also clear that the velocity of the ring will not change unless the vorticity of the ring is spread over a region which can be easily observed by the increase of its radius r. Thus, at this initial stage, the ring is expected approximately to behave as if it were in an ideal fluid. A certain period of time after the ring is generated, the motion becomes turbulent and turbulent diffusion comes into play. At this stage, the diameter of the ring would be expected to increase rapidly as it travels downstream. Eventually, all the kinetic energy of the puff will be transferred to turbulent energy and the ring thus will fade out of sight.

When a circular vortex ring travels along a common axis which coincides with the x-axis, it is evident that the longitudinal velocity component, u, the radial velocity component, v, and the vorticity, ζ, at any point in the field are functions of the longitudinal distance, x, and the radial distance, r.

If the stream function of the motion is Ψ, then the foregoing velocity components may be expressed as

$$u = -\frac{1}{r}\frac{\partial\Psi}{\partial r}, \tag{1}$$

$$v = \frac{1}{r}\frac{\partial\Psi}{\partial x}$$

and the vorticity,

$$\zeta = \frac{\partial v}{\partial x} - \frac{\partial u}{\partial r} \tag{2}$$

$$= \frac{1}{r}\left(\frac{\partial^2\Psi}{\partial x^2} + \frac{\partial^2\Psi}{\partial r^2} - \frac{1}{r}\frac{\partial\Psi}{\partial r}\right).$$

To determine the stream function Ψ, it may be assumed that the flow is given by the line integral of some function around the boundary curve [6], i.e.

$$\int_S (lu + mv + nw)\, ds = \oint_{(c)} (L dx + M dy + N dz) \tag{3}$$

where l,m,n are the direction cosines of the normal to the surface element ds; L,M,N are a set of functions; (c) is a closed curve which lies on the surface of the filament; s is a surface stretched over the curve (c); u,v,w are the corresponding velocity components in the axial, radial, and tangential directions, respectively. Using Stokes' theorem, one finds

$$\oint_{(c)}(Ldx + Mdy + Ndz)$$

$$= \int_S [l(\frac{\partial N}{\partial y} - \frac{\partial M}{\partial z}) + m(\frac{\partial L}{\partial z} - \frac{\partial N}{\partial x}) + n(\frac{\partial M}{\partial t} - \frac{\partial L}{\partial y})]ds \qquad (4)$$

Comparing equations (3) and (4), we obtain

$$u = \frac{\partial N}{\partial y} - \frac{\partial M}{\partial z}$$

$$v = \frac{\partial L}{\partial z} - \frac{\partial N}{\partial x}$$

$$w = \frac{\partial M}{\partial x} - \frac{\partial L}{\partial y} \qquad (5)$$

It is necessary and sufficient that these three functions should satisfy

$$\xi = \frac{\partial w}{\partial y} - \frac{\partial v}{\partial z} = \frac{\partial}{x}(\frac{\partial L}{\partial x} + \frac{\partial M}{\partial y} + \frac{\partial N}{\partial z}) - \nabla^2 L$$

$$\eta = \frac{\partial u}{\partial z} - \frac{\partial w}{\partial x} = \frac{\partial}{\partial y}(\frac{\partial L}{\partial x} + \frac{\partial M}{\partial y} + \frac{\partial N}{\partial z}) - \nabla^2 M$$

$$\zeta = \frac{\partial v}{\partial x} - \frac{\partial u}{\partial y} = \frac{\partial}{\partial z}(\frac{\partial L}{\partial x} + \frac{\partial M}{\partial y} + \frac{\partial N}{\partial z}) - \nabla^2 N$$

They will in any case be indeterminate to the extent of three additive functions, which may be so chosen that

$$-\frac{\partial L}{\partial x} - \frac{\partial M}{\partial y} - \frac{\partial N}{\partial z} = 0 \tag{6}$$

Hence,

$$\xi = \frac{\partial w}{\partial y} - \frac{\partial v}{\partial z} = -\nabla^2 L$$

$$\eta = \frac{\partial u}{\partial z} - \frac{\partial w}{\partial x} = -\nabla^2 M$$

$$\zeta = \frac{\partial v}{\partial x} - \frac{\partial u}{\partial y} = -\nabla^2 N \tag{7}$$

Particular solutions of these equations are obtained by equating L,M,N to the potentials of distributions of matter whose volume-densities are $\xi/4\pi, \mu/4\pi, \zeta/4\pi$, respectively. For the case of a circular vortex ring, in which all vorticity components but that in the direction perpendicular to both x and r vanish, we may thus simply write:

$$N = \frac{1}{4\pi} \iiint_V \frac{\zeta'}{r}\, dx dr d\theta \tag{8}$$

where ζ' is the value of ζ at the point (x', r', θ').

To find the value of Ψ at a point (x,r) due to a single vortex filament of circulation Γ, whose coordinates are (x',r'), we may denote that the element which makes an angle θ with the direction of H may be denoted by $r'd\theta$, and therefore

$$\Psi = -\frac{\Gamma r r'}{4\pi}\int_0^{2\pi}\frac{\cos\theta}{\phi}\,d\theta \tag{9}$$

where $\phi = \{(x-x')^2 + r^2 + r'^2 - 2rr'\cos\theta\}^{\frac{1}{2}}$

If ϕ_1 and ϕ_2 denote the least and greatest distances of the point P from the vortex, respectively, we may write:

$$\phi_1^2 = (x-x')^2 + (r-r')^2$$

$$\phi_2^2 = (x-x')^2 + (r+r')^2$$

Hence,

$$\phi^2 = \phi_1^2\cos^2\frac{\theta}{2} + \phi_2^2\sin^2\frac{\theta}{2}$$

$$4rr' = \phi_1^2 - \phi_2^2 - 2r^2 \tag{10}$$

Therefore,

$$\Psi = -\frac{\Gamma}{8}\{(\phi_1^2 + \phi_2^2)\int_0^{\pi}\frac{d\theta}{(\phi_1^2\cos^2\frac{\theta}{2} - \phi_2^2\sin^2\frac{\theta}{2})^{\frac{1}{2}}}$$

$$-2\int_0^{\pi}(\phi_1^2\cos^2\frac{\theta}{2} + \phi_2^2\sin^2\frac{\theta}{2})^{\frac{1}{2}}\,d\theta\} \tag{11}$$

By means of Landen's transformation, the above expression may be rewritten into a simple form:

$$\Psi = -\frac{\Gamma}{2\pi}(\phi_1 + \phi_2)[F_1(\lambda) - E_1(\lambda)], \tag{12}$$

where $$\lambda = \frac{\phi_1 - \phi_2}{\phi_1 + \phi_2}.$$

In considering the case of an isolated vortex ring, the dimensions of whose cross section are small in comparison with the radius r of the ring, the ratio ϕ_1/ϕ_2 is small for points in or near the substance of the vortex, and λ is near unity. We then have

$$F_1(\lambda) = \frac{1}{2}\ln\frac{4(\phi_1 - \phi_2)^2}{\phi_1\phi_2}, \tag{13}$$

and $$E_1(\lambda) = 1.$$

At points within the substance of the vortex, the value of Ψ is of order $\Gamma r \ln\frac{r}{\varepsilon}$, where ε is a small quantity compared with the dimensions of the section.

For circular section, neglecting the variations of r and ζ over the section, we may obtain from Equations (12) and (13);

$$\Psi = -\frac{\zeta r}{2\pi}\iint\left(\ln\frac{8r}{\phi_1} - 2\right)dx'dr', \tag{14}$$

or in polar coordinates,

$$\Psi = -\frac{\zeta r}{2\pi}\int_0^a \int_0^r (\ln\frac{8r}{a} - 2)s'ds'd\phi, \tag{15}$$

where a is the radius of the circular section and is much less than r.

Hence,

$$\Psi = -\frac{1}{2}\zeta r a^2\{\ln\frac{8r}{a} - \frac{3}{2} - \frac{1}{2}\frac{s^2}{a^2}\}, \tag{16}$$

for any point (s,β) inside the section. The only variable part of Equation (16) is the last term; this shows that the stream lines within the section are concentric circles, and the velocity at a distance s from the center is $\frac{1}{2}\zeta$ s.

The energy of the vortex ring is defined as

$$T = \pi\rho \iint (u^2 + v^2) r dr dx$$

$$= \pi\rho \iint (v\frac{\partial\Psi}{\partial x} - u\frac{\partial\Psi}{\partial r}) dx dr$$

$$= -\pi\rho \iint \Psi\zeta\, dx dr. \tag{17}$$

By substitution of Equation (16), Equation (17) becomes

$$T = \frac{\Gamma^2 r\rho}{2}\{\ln\frac{8r}{a} - \frac{7}{4}\}. \tag{18}$$

The impulse of the puff is

$$P = \frac{1}{2}\rho \iint (ru - xv)\ \zeta r dr dx$$

$$= \pi\rho \iint \zeta r^2 dr dx.$$

Since it is assumed that the radius of the ring does not change much at this initial stage and that the vorticity is a constant throughout the motion, the above relation is simplified, using the Stokes' theorem, to

$$P = \pi\rho\Gamma r^2 \tag{19}$$

The velocity of advance of the ring is given by Turner [10] and is due to Sir Wm. Thomson

$$V = \frac{\Gamma}{4\pi r}\{\ln \frac{8r}{a} - \frac{1}{4}\}. \tag{20}$$

From this expression, it is very clear that the ring will not change its velocity unless the vorticity of the ring is spreading over a region which can be easily observed by the increase of r. In an ideal fluid, however, such a spreading phenomenon does not exist. Even in laminar motion, such a spread will be insignificant.

II. ANALYTICAL APPROACH OF THE MOTION OF THE RING IN THE TURBULENT STAGE

A certain period after the ring is generated, it is expected that turbulence will start. At this stage, the turbulent diffusion comes into play and the diameter of the ring will increase noticeably as the ring travels downstream.

It was noticed as early as 1876 by Reynolds that the impulse of vortex ring proceeding in a real fluid domain is substantially constant for a considerable distance. It seems reasonable to assume that the relations like Equations (18), (19), (20) would be approximately valid in a viscous fluid [10].

If Equation (19) is applied to the motion in the turbulent region, it would bring about the conclusion that the impulse P would increase with the time as the ring travels, since it is assumed that the circulation Γ is a constant throughout the motion. It is, therefore, immediately clear that the relation (19) and its corresponding formulae like Equations (18) and (20) which were derived from ideal fluid assumptions cannot be applied to the motion of turbulent state, and those relations are valid only when the motion is approximately laminar as mentioned in the previous section.

Early experiments with isolated masses of buoyant fluid of constant total buoyancy in unstratified surroundings

(Scorer [7], Woodward [8], Turner [9], Richards [4]) showed that each isolated mass obeyed the equation,

$$r = \frac{x}{n} \tag{21}$$

where x is the distance traveled by the leading extremity of the turbulent region, 2r is the greatest horizontal dimension of the turbulent region, and n is a numerical constant for each isolated mass.

Previous work by Richards [4] also showed that the relation $d\{\rho r^a (dx/dt)\}/dt = Cmg$ describes the motion of the buoyant mass, where t is time, ρ is the density of the fluid, g is the gravitational acceleration, C is a numerical constant, and m is the mass excess.

The general case of turbulent puff motion is so complicated that it is suggested to describe the motions of the ring with the following restrictions:

(1) Any external force acts only in the direction of the ring motion as a whole;

(2) The external and internal densities are equal;

(3) The surrounding fluid field is unstratified and is stationary except when the particles are associated with the motion of the ring itself.

By assuming that the vortex motion follows some kind of similarity law of decay, one may treat the ring in the following way:

If it is assumed that the velocity distribution in the ring at this stage follows a linear similarity law, then the ring should follow the linear relation resulting from the experiments of Turner [9], Scorer [7], and Richards [4], i.e.

$$R = \frac{X}{n} \qquad (22)$$

For a ring emitted from an orifice of finite radius, Equation (22) becomes

$$X = n(R-R_0), \qquad (23)$$

where X is the non-dimensional distance traveled by the leading extremity of the ring, R is the non-dimensional radius of the ring in the plane normal to the ring-axis, R_0 is the non-dimensional radius of the outlet, and n is a numerical constant.

It is also assumed that the fluid density may be taken as substantially unvaried through the travel distance of the ring, and that the fluid viscosity is irrelevant to the motion. Then, the velocity of advance of the ring (leading extremity) may be given as

$$V^2 = n_1 \frac{Fr}{m}, \qquad (24)$$

from dimensional considerations. Under the assumption that the pseudo-force acting on the ring and the density are held constant, V is a function of R only.

By the first assumption, and that the impulse of the ring is in the direction of the axis of motion of the ring, the magnitude of the impulse is therefore approximately proportional to the product of a characteristic velocity with the density of the fluid and the cube of a characteristic linear dimension of the ring. The relation may be expressed as

$$P = C_1 \rho R^3 \left(\frac{dX}{dt}\right), \tag{25}$$

where C_1 is a proportional constant, R is the nondimensional radius chosen as the characteristic linear dimension of the ring, and $\frac{dX}{dt}$ is the velocity of advance of the ring taken as the characteristic velocity.

Since the force acting on the ring should be equal to the rate of change of the impulse, we may write

$$\frac{d}{dt}\left\{C_1 \rho R^3 \left(\frac{dX}{dt}\right)\right\} = F. \tag{26}$$

With the restrictions (2) and (3) on page 12 and the initial condition of zero momentum, Equation (26) may be integrated with respect to time to give

$$C_1 \rho R^3 (\frac{dX}{dt}) = Ft.$$

The fact that the pseudo-force is taken to be constant will be discussed later.

Let $I = Ft$ and $C = 1/C_1$, then Equation (26) becomes

$$R^3 (\frac{dX}{dt}) = CI/\rho. \tag{27}$$

Using Equation (23) and integrating Equation (27) with respect to time, we obtain

$$Z/n^3 = CI\ t/\rho + C'. \tag{28}$$

At $x = 0$, we have $t = t_0$, so Equation (28) becomes

$$Z/n^3 = CI\ (t - t_0)/\rho \tag{29}$$

where Z is $(X^4/4 + X_0X^3 + 1.5X_0{}^2X^2 + X_0{}^3X)$, I is the momentum, and C is a numerical constant determined experimentally.

Let dI/dt be the flux of linear momentum through the plane perpendicular to the ring-axis. Then

$$\frac{dI}{dt} = \int \rho V|V| dA, \tag{30}$$

where V is the velocity of advance of the ring given by $\frac{dX}{dt}$, and dA is the element of area. The integral of Equation (30) may be approximated by $\rho AQ|Q|/A^2$, in which A is the sectional area of the ring in the plane normal to the ring-axis, and Q is the volume rate of change of the ring, which is given by VA. By the substitution of R, V, A, and Q, Equation (30) becomes

$$\frac{dI}{dt} = \rho Q|Q|A/A^2$$

$$= \pi\rho R^2 (\frac{dX}{dt})^2. \qquad (31)$$

The integration of Equation (31) with respect to time, using zero initial momentum, yields

$$I = \rho\pi R^2 (\frac{dX}{dt})^2 t \qquad (32)$$

CHAPTER III

EXPERIMENTAL METHOD

I. THE EXPERIMENTAL FACILITIES

The experimental facilities of this thesis were installed in a confined room. Through the entire laboratory work the following facilities were used: two different hot-wire anemometer sets, a smoke ring tunnel of four feet of plastic pipe with I.D. 8-3/4 inches, ring generating parts composed of a constant speed motor and a driving system. An oscilloscope Tektronix type 561 and a Tektronix C-12 Polaroid camera were used as recording devices; polaroid film of speed 3000/type 47 was used. A carriage assembly was designed for moving and positioning the hot-wire probe, and a table-type stop watch was used for the timing. The hot-wire probes were cleaned with alcohol at intervals.

Plate 1 shows a front view of the tunnel and chamber, and Plate 2 is for the ring generating parts. These ring generating parts and the tunnel were designed in such a manner that they were capable of producing viscous rings of approximately the same general characteristics repeatedly.

The Hot-Wire Anemometers

Two sets of hot-wire anemometers of different designs have been used for the experiment. The first was a constant-current anemometer, Flow Corp. HWB 3 type. The sensor of this instrument is a thin tungsten wire of 0.004 inches long with a diameter of 0.00015 inches. The wire was heated by a constant electrical current. The measurement of local velocity is based on the measure of the change in electrical resistance of the hot-wire due to the cooling effect of the surrounding fluid flow.

The second was a constant temperature hot-wire anemometer, DISA 55A01 type, which has the principle of measurement depending on the cooling effects of an electrically heated wire, as measured by the heating current required to maintain the wire at a fixed constant temperature. A platinum-plated tungsten wire was selected as the hot-wire, which had a length of 1.2 mm and diameter 5μ. The resistance of the wire at 20°C is $3.5 \pm^{0.7}_{0.5}$ ohm.

The Experiment Tunnel

A four-feet long, 17½ inches diameter transparent plastic tube was used as the experiment tunnel. It was required that the viscous ring had to proceed downstream without an external effect such as air currents. In order to keep the viscous rings from the disturbances caused from the air currents, and to avoid any possible effect on the ring motion by the buildup pressure in the tunnel, only the downstream end of the tunnel was open to the room air.

The experiment tunnel was chosen to be circular since it was desired to generate circular rings. The tunnel diameter should be large enough to ignore the effects of friction between the ring and tunnel wall. Plastic was selected as the material for the tunnel to allow for observation of the motion. The test-section of the tunnel was located such that no exit effects were present.

The tunnel was connected to the outlet of the ring generating chamber concentrically. On the top of the test section of the tunnel, a guide was constructed so that the hot-wire probe could move freely in the longitudinal direction.

Ring Generating Parts

Ring generating parts consisted of a cylindrical chamber, a pusher, a lever with a calibrated driving spring, and a constant speed motor with a gear box and a calculated cant on its pivot.

The cylindrical chamber, as shown in Plate 3, had a length of two inches and an inner diameter of two inches. On the back side, it was covered by a rubber membrane. The rubber membrane was of hygienically pure latex 5" x 5", which was very thin (0.007 inches) so that the bending stresses in the membrane may be neglected. Also, it was age resistant and was hard to tear. At the front end of the chamber, a circular hole of diameter 1/2 inch was open to the experiment tunnel as the outlet of the viscous ring. The circular hole was rounded in the inside edges but was flush on the outside plate.

A constant speed motor of 30 RPM was equipped with a cant on its pivot. The cant was designed to complete the motion of push in $\frac{1}{40}$ sec.

As the portion of contact of the cant with the pushing lever rod, plastic rollers were used to minimize the friction.

The viscous ring was generated by the pushing of the rod against the membrane of the cylindrical chamber. The lever system was powered with a calibrated driving spring and the constant speed motor. The pushing was executed in the interval of no less than 20 seconds.

The Carriage Equipment

The carriage assembly was constructed so that the hot-wire probe could be moved in two directions: horizontally, in the advance direction of the viscous ring, by positioning the hot-wire rider carriage with an accuracy of $\pm\frac{1}{32}$ inch; vertically by positioning the hot-wire rider along the carriage with an accuracy of $\pm\frac{1}{64}$ inch for an exact position for the hot-wire probe.

The carriage was so placed that the hot-wire ran parallel with the axial line of the tunnel (the average axis of the viscous rings). The carriage base was made of heavy steel to minimize the undesired vibration of the hot-wire probe which might be absorbed from the carriage assembly.

II. CALIBRATION OF THE HOT-WIRE

The mean flow velocity can be directly observed from the D.C. voltage meter of the constant temperature hot-wire anemometer after ploting the calibration curve of one hot-wire. For the constant current hot-wire anemometer,a D.C. current meter was used.

In order to measure the local velocity with proper accuracy, an experimental calibration curve is required for each hot-wire, because the hot-wires may not be identical in their characteristics.

In the construction of the calibration curve, the hot-wire probe and the pitot tube should be mounted closely in a flow region concerned so that the effect of velocity distribution may be neglected. The bridge D.C. voltage for the constant temperature anemometer (or current for the constant current anemometer) is plotted against the flow velocity measured by the pitot tube. The calibration curve has the square of the voltage (or current) as the ordinate and the square root of the velocity (or the product of pressure and velocity) as the abscissa.

For the plot of calibration curve in the laboratory, the following equipment was used: A micromamometer, Flow Corp. MM-3 type, for which the accuracy of reading is ±0.0002 in. corresponding to six millionths of one psi. with butyl alcohol as the liquid (ρ = 0.81 gr/cc); a standard pitot-static tube;

a small centrifugal air blower of 3200 RPM, whose outlet velocities were controlled by an adjustable door at the inlet; with the door open fully the velocity recorded in the calibration pipe was 0.298 ft/sec. The calibration windtube was a 4½ feet long plastic pipe with 3-3/4 inches I.D.

A triple metal grid was mounted at the inlet portion of the wind tube to generate downstream turbulence. The metal grid was necessary since the normal flow was laminar.

For the calibration curve, the measurement of velocity was carried out at 40 mesh lengths downstream, where an approximately fully-developed turbulent flow could be obtained. During the calibration process, great difficulties were encountered in reading the micromamometer at these very low velocities. The resulting curve could only be used as a guide for justifying the similarity in characteristics of two different hot-wires in general.

One plausible way of calibrating the hot-wire at this very low velocity range would be the towing method. In this process, the hot-wire probe was mounted on a carriage and towed through a long chamber of stagnant air with different constant-speeds. The corresponding bridge D.C. voltage (or current) would then be plotted against the measured speed for the curve. This equipment was not available at the time of the experiment.

In describing the local characteristics of the viscous ring, a non-dimensional form was used. The coordinates were also expressed in non-dimensional form. The non-dimensional axial distance, x/D from the outlet of the chamber was denoted by X, and the non-dimensional radial distances, r/D from the axial line (ring-axis) in one direction (upward) and in the opposite direction (downward) were denoted by (+)R and (-)R, respectively. The x, in cylindrical coordinate system with the origin at the center of the outlet, is the distance measured downstream, r is the radial distance from the ring-axis, and D is the diameter of the outlet of the chamber.

For the non-dimensional form, the calibration was modified as the following: Along the ring-axis the velocities were measured as a reference velocity at each measuring section, which is perpendicular to the ring-axis. At each section, the velocities were converted by multiplying by the ratio of the reference velocity to the velocity at the point where the reference velocity was obtained. By the conversion, it was expected to get a rather reliable and uniform distribution of velocities. The reasons for the above conversion were based on the fact that at the beginning of the measurements the cold resistance of the hot-wire (or wires) may vary slightly; during the measurement the room temperature may also change in the range of about 3°F; and the measuring technique at each time might not be identical. In other words, the above variations may cause some difference in the readings on a day-to-day basis, and the non-dimensionalizing technique should be able to eliminate the errors.

III. MEASUREMENT OF MEAN VELOCITY

Since it was assumed that the viscous ring consisted of statistically concentric circles, i.e., axisymmetric rings, the measurement of local mean velocity at each point in the field was conducted in one direction through the vertical sectional areas of the viscous ring.

Measuring devices consisted of the following equipment: two hot-wire anemometers, a Tektronix Oscilloscope, and a still camera to record the output of the hot-wire anemometer. The camera was the Tektronix type C-12 camera, which has been specifically designed for photographing an oscilloscope screen so the image is not reversed.

The mean flow velocity can be read from the bridge D.C. voltage (or current) meter which was built in the anemometer as an integrated part, and the read-out is a function of voltage (or current). For the low velocity, increased sensitivity could be obtained by making use of the oscilloscope with fixed bias voltages in the hot-wire anemometer DISA 55A01, which was established by using a D.C. compensator between the output of the anemometer and the input of the oscilloscope.

The following precautionary steps had been taken during the velocity measurement: Any exhaust fans and air conditioning and ventilation units were turned off to insure that the air currents were not affecting the viscous ring motion in the tunnel. The hot-wire was held perpendicular to the advance direction of the viscous ring, i.e., the stream velocity vector of the ring was approximately perpendicular to the axis of the hot-wire filament; the viscous ring was generated at no less than 20 sec. intervals to ensure the statistically similar structure in the tunnel.

To determine the effect of the puffing interval on the structure of the ring, wide ranges of puffing intervals had been tested before any experimental data were collected. From these testing results, it was found that a minimum puffing interval of 20 seconds was justified. During the testing period, it was also found that the results were quite randomly distributed. A successful result was obtained in the following way. By consecutive puffing of the rings, it was possible to obtain a certain disturbance of the fluid in the tunnel for which statistically steady results were observed. According to the experimental results, the standard deviations of these variations were around zero. This technique was conducted first at $x/D = 10$ along the axis of symmetry, and then at several downstream stations.

The experimental data were first collected by the constant current hot-wire anemometer, Flow Corp. HWB 3 and the following difficulties were encountered.

1. The out-put signals from the constant current hot-wire anemometer were the time derivatives of the velocity signals. It composes both positive and negative portions on the oscilloscope screen and, hence is very difficult to integrate;

2. At low frequency operation (such as this experiment), minor disturbances may easily burn out the hot-wire.

The hot-wire used was a 0.0004 inch long tungsten wire of 0.00015 inch diameter. The operating resistance ratio of 1.4 - 1.2 was used.

These difficulties were resolved when the constant current hot-wire anemometer was replaced by a constant temperature hot-wire anemometer, DISA 55A01. By using the new constant temperature set, the D.C. output terminal on the front panel gave directly the integrated signal on the screen of the oscilloscope; the magnitude of this positive signal is proportional to the local mean velocity of the motion. The local mean velocity is obtained by using the linear relationship between the square of D.C. voltage and the square root of the flow velocity. The operating resistance of the hot-wire with the constant temperature set was about 6.3 ohms. The ratio of cold resistance to operating resistance of the wire was 1.8, and was used throughout the experiments. As a sensor, a 1.2 mm long platinum-plated tungsten wire of 5μ diameter was used. The probe was a hot-wire of type DISA 55A25.

As a recording device, polaroid films of speed 3000 type 47, were used. Photographs were taken at the time scale 0.5 - 2 sec. per centimeter of the oscilloscope screen with the aid of a triggering device. The aperture control and shutter speed of the camera were f/1.6 and B, respectively.

Throughout the experimental work, the maximum fluctuation of the temperature in the tunnel was about 3°F. The corresponding resistance fluctuation of the hot-wire was about 2.23×10^{-4} ohms per degree F. This value was considered to be small enough to neglect any effect of temperature fluctuations in the normal range.

At each measuring position, the elapsed time of leading extremity of the viscous ring was measured by means of a table-type stop watch. The stop watch was electrically connected to the ring generator to provide a simultaneous motion. The ring motion was generated behind the outlet of the chamber. Therefore, the actual elapsed time from the outlet may be given as the following form:

$$t = t' - t_0$$

in which t' is the elapsed time measured from the assumed position as the starting point of ring motion, and t_0 is the time interval of ring motion between the aforementioned position and the center of outlet corresponding to the origin of coordinates used through this thesis.

CHAPTER IV

ANALYSIS OF DATA

I. ESTIMATES OF RING RADIUS

The experimental data of local mean velocities at each testing section are shown in Figure 1 as the graph of dimensionless velocity against dimensionless radial distance.

Observation of the resulting curves in Figure 2 shows that the radial distance R is an exponential function of the velocity and may be expressed as the following form:

$$R = \frac{1}{U} \text{EXP} \left(- \frac{1}{U_0 - U}\right)$$

in which R is the radial distance, U is the velocity at radial distance R, and U_0 is the velocity along the ring-axis. It is easily seen that the radial distance R is roughly equal to the radius of the ring composed of the points with velocity U around the ring-axis. The radii corresponding to different velocities were measured from the velocity profile. The graphs of 2R against X were then plotted, and the slope of the graph n/2 was given as n-value. A typical example of such a graph at $U/U_0 = 0.5$ is shown in Figure 3. As shown in Figure 2, the value of n suddenly changed as the ring travels downstream along its axis. This sharp change took place around X = 20.

This fact, which was also observed by Richards, in puff motion [4] indicates the increase in radius of the ring with the forward movement of the ring. This result clearly solidifies the prediction in Chapter II with a physical meaning to be mentioned. These two different regions formed by the two distinguishably different n-values are denoted by region I and II, which, as mentioned in Chapter II, are physically the initial region and the turbulence region, respectively.

In the region I, the increase of radius with distance is insignificant, and the only contribution to diffuse the ring into the surroundings is probably the molecular agitation. Since the scale of molecular diffusion is very small compared with that of the turbulent diffusion when it started, it is therefore reasonable to neglect the effect of diffusion in this initial region. The motion in this region can thus be treated approximately as a laminar motion and the ring is expected to behave as if it were in an ideal fluid.

In the second region, region II, the increase in radius of the ring is significant. It is easily visuable that the flow is dispersed, and the effects of turbulent diffusion are noticeable. The region II may therefore be regarded as a turbulent region. By restriction (2) in Chapter II, the velocity of advance of the ring will decrease as the ring radius increases, and the fluid mass involved with the ring motion will increase correspondingly. It seems reasonable.

to assume that the force acting on the ring is constant throughout the distance traveled by the ring. This assumption is verified by the experimental data as will be shown later.

As predicted in Chapter 2, the viscous ring motion will generally follow the linear relation

$$X = nR,$$

and the n-value may be obtained from the experimental data as the slope of the graph of distance X plotted against the radius R. In the two regions mentioned above, distinguishably different n-values are expected. These values were obtained by a least square fit of a straight line into our measured data and the resulting values are:

$n = 281$ for the region I (laminar),

$n = 41$ for the region II (turbulent).

II. ADVANCE VELOCITY OF RING

It is assumed that the relationship between the distance, X traveled by the leading extremity of the ring and the elapsed time t follows a quadratic form,

$$t = aX^2 + bX + c,$$

in which the coefficients a, b, and c are to be determined by the least square polynomial approximation [11]. As shown in Figure 4, this approximation yields

$$t = 0.0011X^2 + 0.0011X + 0.0803. \qquad (33)$$

Hypothetically, for our experiment, the motion of the ring should be initiated at some virtual origin which can be determined by taking $X = X'$ where $t = 0$. The time t_0 required for the ring to travel the distance X' between the two origins is obtained from the Equation (33) as $t_0 = 0.0803$ sec.

The advance velocity of the ring may also be determined from Equation (33), which gives

$$\frac{dX}{dt} = (0.0022 \times +0.0011)^{-1}. \qquad (34)$$

Equation (34) is plotted as a function of time, t, in Figure 5. It is seen that the velocity of advance of the ring varies only slightly with time in the neighborhood of the elapsed time $t \leq 0.05$ sec. in Figure 5. The period followed by $t = 0.05$ sec. corresponds to the region II (turbulent). Under the assumption of constant pseudo-force acting on the ring, it is noted that an increase in radius (or mass for constant density) of the ring is a necessary consequence of the slight change in the velocity with time.

In the region II (turbulent), the local mean velocity is also shown in Figure 5. This Figure also shows a slight change of velocity with elapsed time similar to that of the advance velocity of the ring.

III. LINEAR MOMENTUM WITH DISTANCE

Equation (32),

$$I/\rho = \pi R^2 t \left(\frac{dX}{dt}\right)^2, \tag{32}$$

is plotted in Figure 6 for both the laminar and turbulent motions of the ring. In the turbulent region the plot is a straight line which indicates a linear relation between the increase of linear momentum and elapsed time. In the laminar region the plot is irregular and shows a decrease in linear momentum with time. This is a further indication of the two distinct regions. Since Equation (32) is derived for the turbulent region, it should not be applicable to the first region as they are governed by two different laws.

The change of the linear momentum may be interpreted as follows:

In the laminar region, the circulation is so highly concentrated that the angular momentum near the vortex filament is preserved throughout the laminar region. At the point of transition where turbulence starts, the cross section of the ring increases. As a result, the concentration of the circulation decreases, and the angular momentum transfers to the form of the linear momentum in the x-direction. The plots in Figure 6 are the result of the calculation of the linear momentum in the x-direction. In the turbulent region, the linear momentum increases as the angular momentum decreases.

The slope of either plot in Figure 6 (which is the derivative of the linear momentum with respect to elapsed time) may be regarded as a "pseudo-force" acting on the ring mass. Thus, it is clear that from the examination of Figure 6 that the pseudo-force acting on the ring in the turbulent region is constant in the x-direction. This result is in exact agreement with the assumption of constant pseudo-force acting on the ring.

The calculation of the linear momentum from Equation (32) was also attempted in the laminar region.

This calculation results in a plot which shows that I/ρ decreases irregularly with elapsed time. Furthermore, the value of I/ρ for the laminar region does not correspond to the value of I/ρ for the turbulent region at the point of transition. Since the turbulent region behaves as one might expect, it follows that this calculation for the laminar region is invalid and has no physical significance.

Therefore, it is concluded that Equation (32) is applicable only to the turbulent region, whereas Equation (19), which was derived from an ideal fluid, describes the laminar region.

The values of Z/n^3 and $I(t - t_0)\rho$ in Equation (29) were calculated for each measuring section. These results are shown in Figure 7, in which the line represents Equation (29), and the slope of the line gives the value of C of Equation (29). It is seen that C-value of 0.011 for the viscous rings is much smaller than that of an axial puff, i.e. C = 0.25 by Richards.

CHAPTER V

CONCLUSIONS

This study was conducted to investigate the characteristics of the smoke ring which travels horizontally in an experiment tunnel. The following conclusions were drawn from the results:

(1) The linear relationship of the ring dimension to the distance it traveled bears the form $x = nr$, which was introduced by the previous workers in this field in studying various types of puff motion, and is applicable to the smoke ring in describing its motion. The flow field is clearly distinguished into two different regions, and they are named in this study as the "laminar" ($x/D \lesssim 20$) and "turbulent" regions ($x/D \gtrsim 20$), respectively. The values of n were found to be 281 and 41 for the laminar and turbulent regions, respectively.

(2) The ring increases its size mainly by turbulent entrainment, and the increase in size is nearly linear with distance.

(3) In the "turbulent" region, the angular momentum gradually transfers to the linear momentum in the longitudinal direction with the increase of elapsed time, and the relation between the momentum and time was fairly represented by a straight line drawn through the experimental data as shown in Figure 6. This implies that the pseudo-force acting

on the ring remains constant with elapsed time, and confirms the assumption. Although the assumption of constant circulation was not directly verified in this experiment, it is clearly seen that the relation $P = \pi\rho\Gamma r^2$ suggested by Lamb [5] cannot be applied to the turbulent region.

(4) The numerical constant C introduced by the previous studies in puff motions with the equation of the form $d\{\rho r^a(dx/dt)\}dt = Cmg$ is also obtained in this study. However, the C-value of 0.011 for the smoke ring is much less than the value of 0.25 which is obtained for a puff motion by Richards [4].

REFERENCES

[1] Bowen, E. G. *Austr. J. Sci. Res.* A. Vol. 3, p. 193.

[2] Turner, J. S. "On the Collision in Turbulent Clouds," *Jour. of Fluid Mech.*, Vol. 1, 1956, p. 16.

[3] Grigg, H. R. and R. W. Stewart. "Turbulent Diffusion in a Stratified Fluid," *Jour. of Fluid Mech.*, Vol. 15, 1963, p. 174.

[4] Richards, J. M. "Puff Motions in Unstratified Surroundings," *Jour. of Fluid Mech.*, Vol. 21, part 2, 1965, p. 97.

[5] Lamb, H. *Hydrodynamics*, sixth edition. Dover, p. 202.

[6] Streeter, V. L. *Fluid Dynamics*. McGraw-Hill, p. 185.

[7] Scorer, R. S. "Experiments on Convection of Isolated Masses of Buoyant Fluid," *Jour. of Fluid Mech.*, Vol. 2, 1957, p. 583.

[8] Woodward, B. *Quart. Jour. Roy. Met. Soc.* Vol. 85, 1959, p. 144.

[9] Turner, J. S. "The Dynamics of Spherical Masses of Buoyant Fluid," *Jour. of Fluid Mech.*, Vol. 19, 1964, p. 481.

[10] Turner, J. S. "Buoyant Vortex Rings," *Proc. Roy. Soc.* A. 239, 1957, pp. 61.

[11] Bennett, C. A. and N. L. Franklin. *Statistical Analysis in Chemistry and Chemical Engineering*. Wiley, p. 245.

APPENDIX

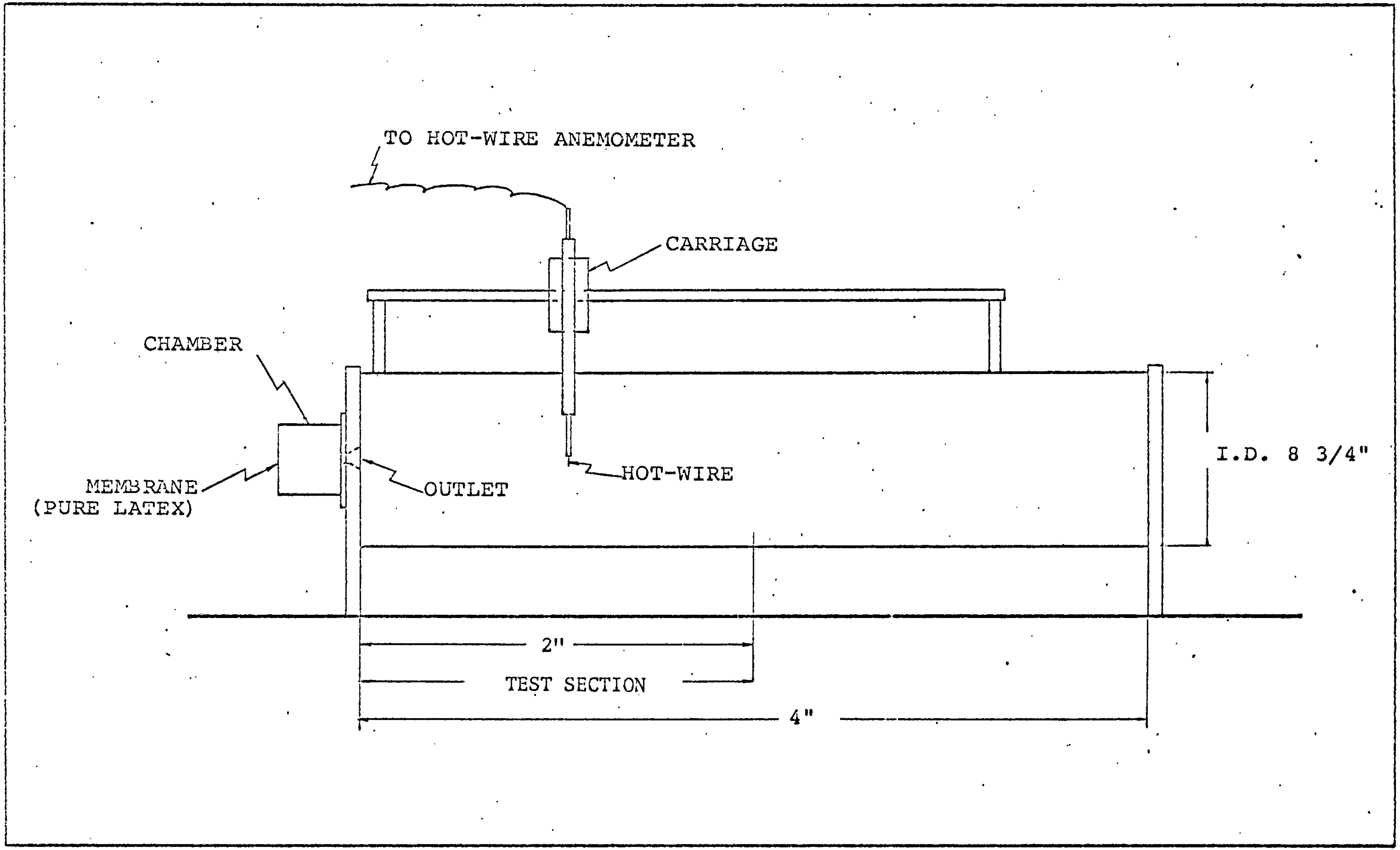

PLATE 1. EXPERIMENT TUNNEL AND CHAMBER

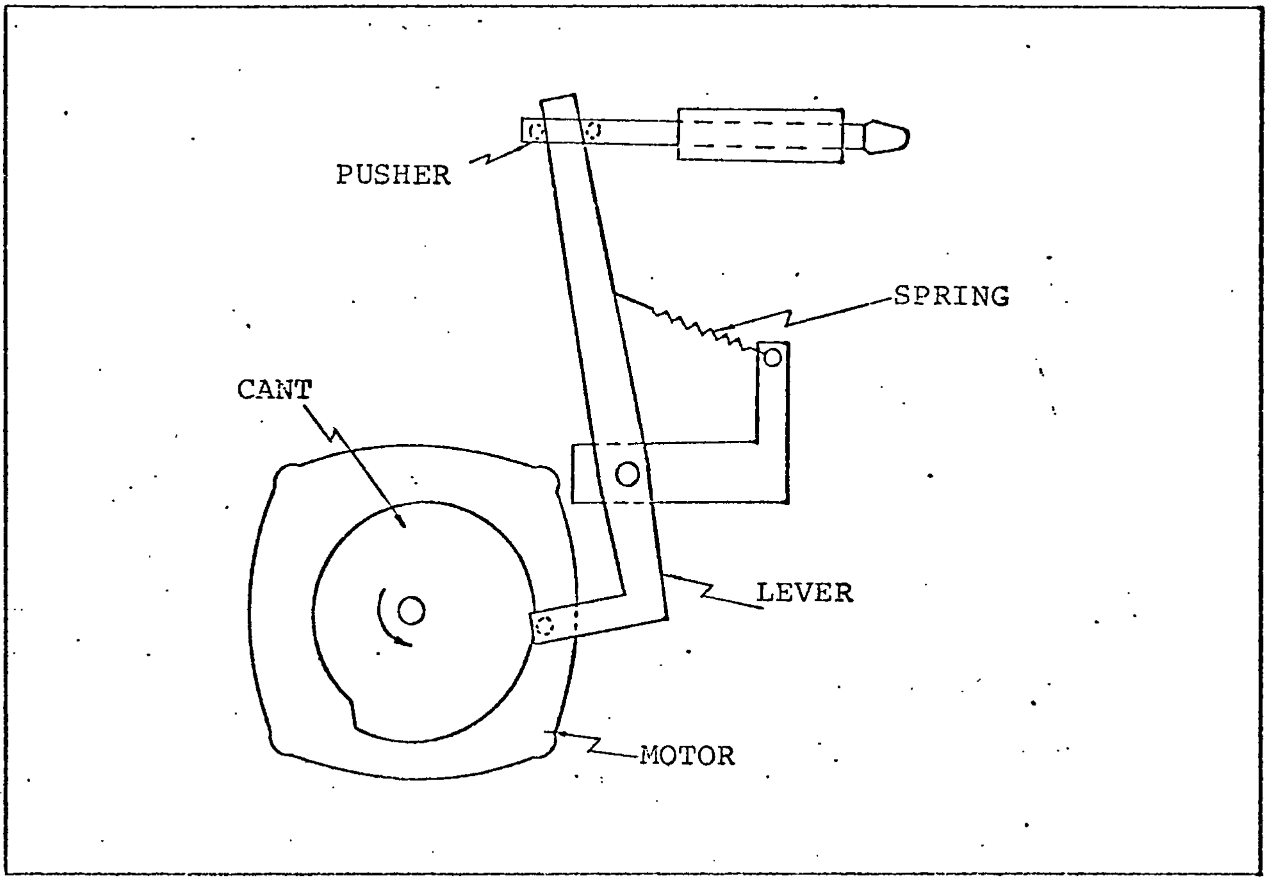

PLATE 2. SCHEMATIC DRAWING OF THE RING GENERATING PARTS

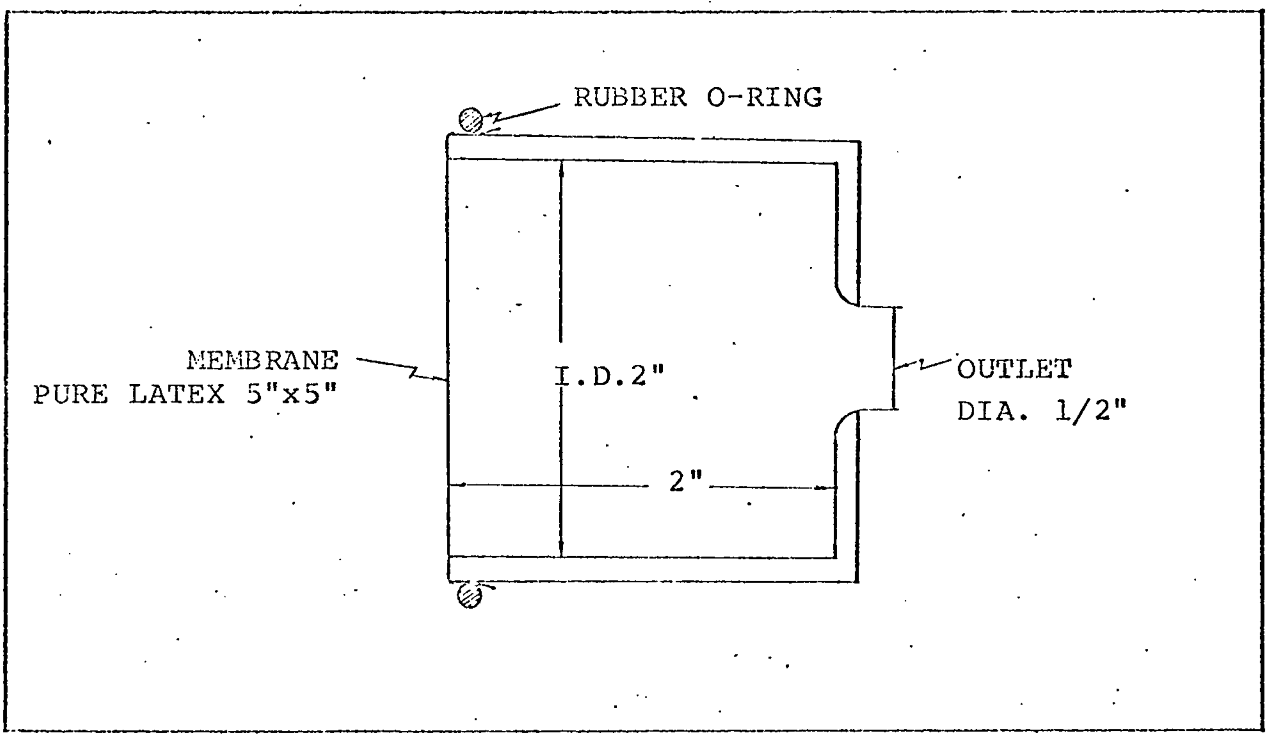

PLATE 3. SCHEMATIC DRAWING OF THE SMOKE RING CHAMBER

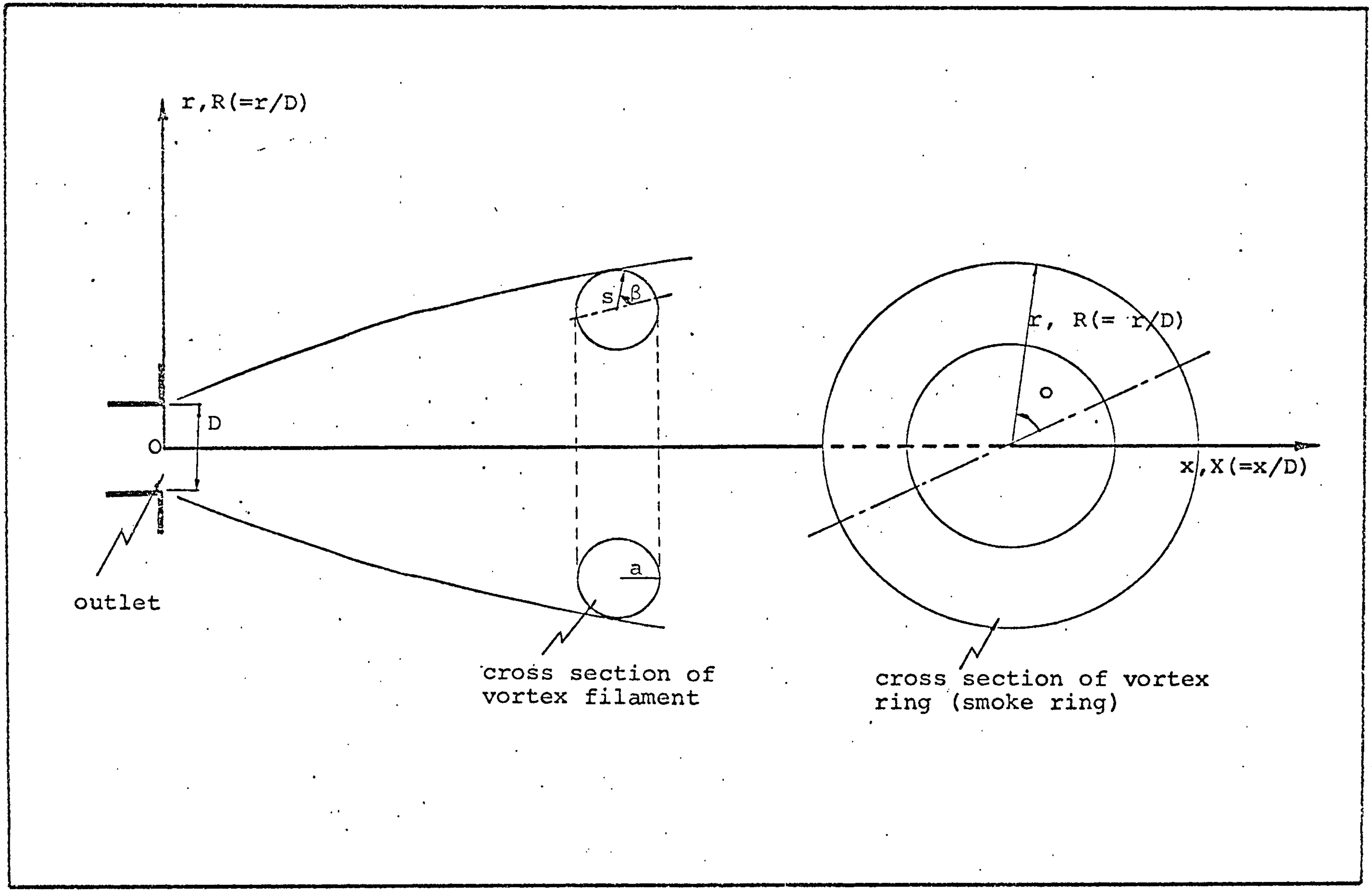

FIGURE 1. DEFINITION SKETCH OF COORDINATE SYSTEM

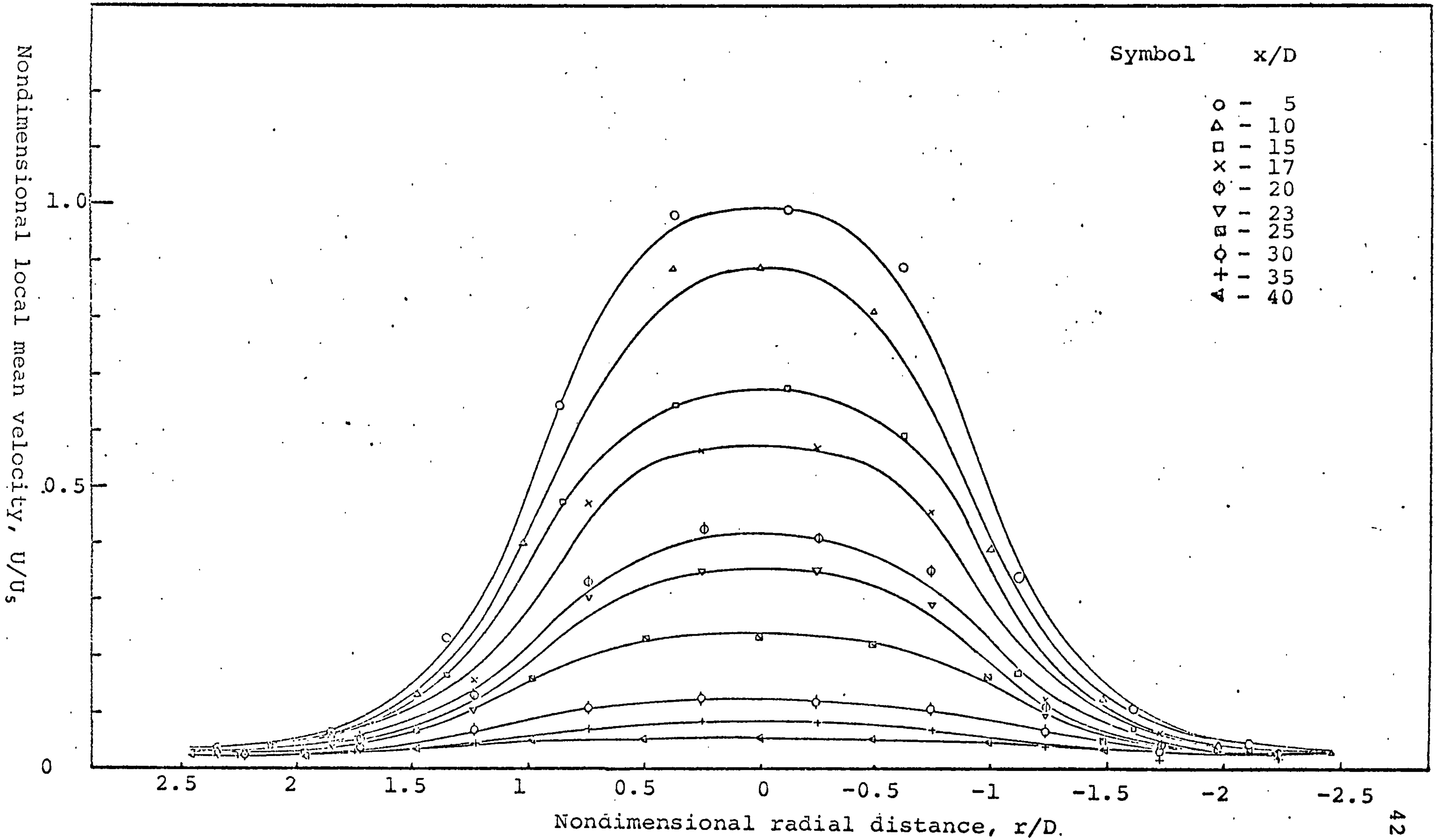

FIGURE 2. LOCAL MEAN VELOCITY AT EACH MEASURING SECTION.

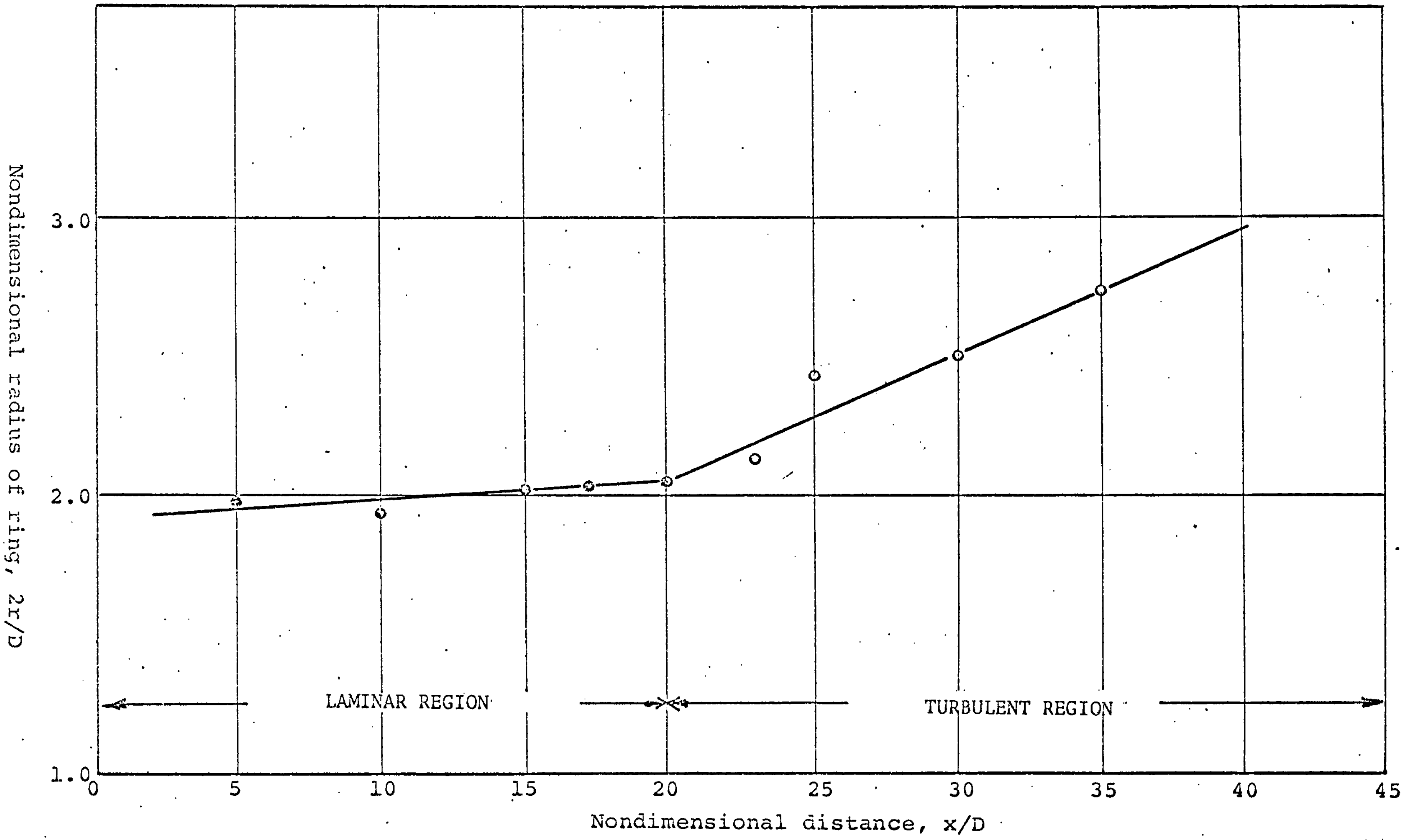

FIGURE 3. CHANGES OF RADIUS OF RING WITH DISTANCE, x/D AT $U/U_0 = 0.5$.

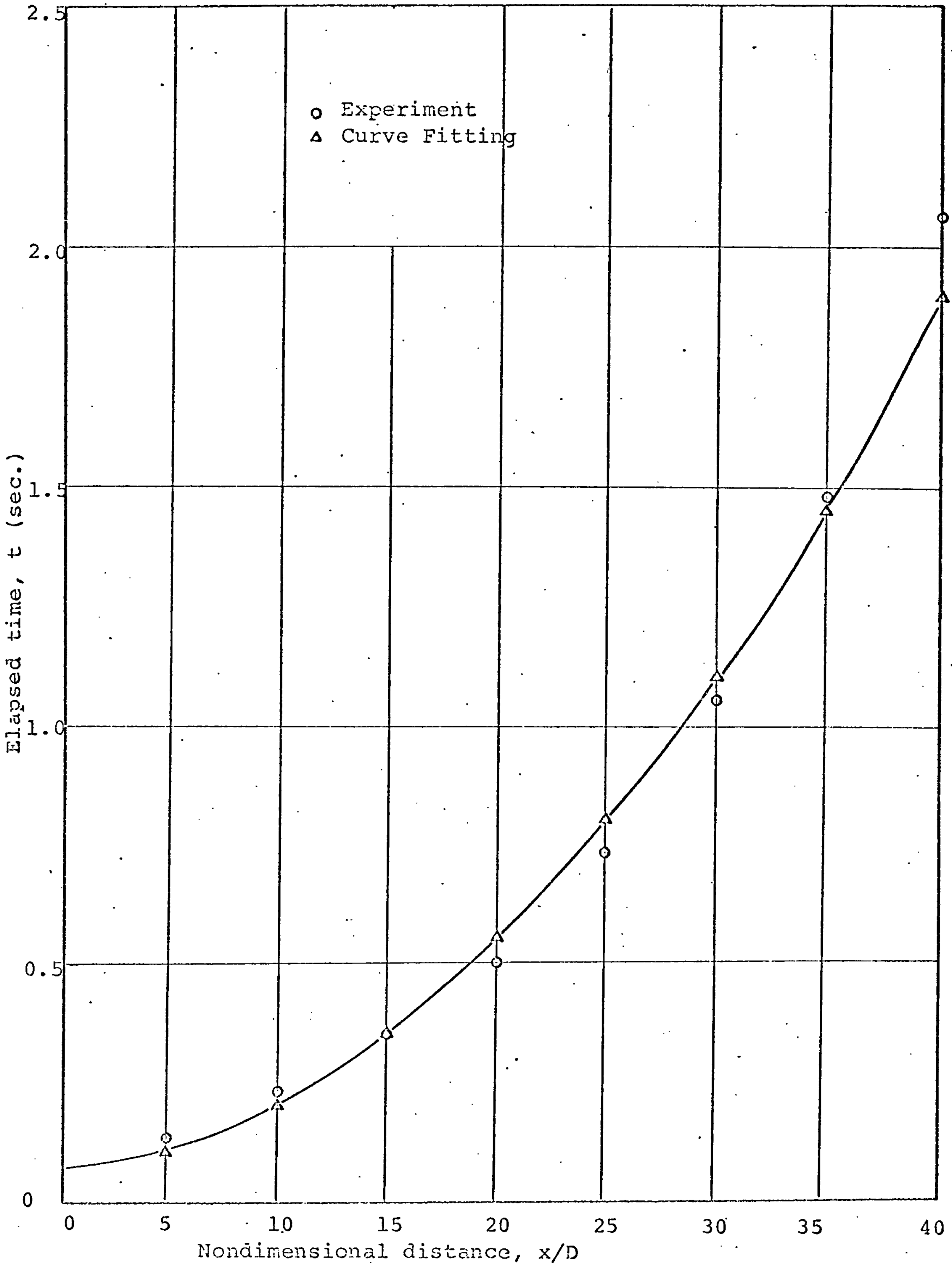

FIGURE 4. RELATIONSHIP BETWEEN ELAPSED TIME, t AND DISTANCE x/D TRAVELLED BY A RING

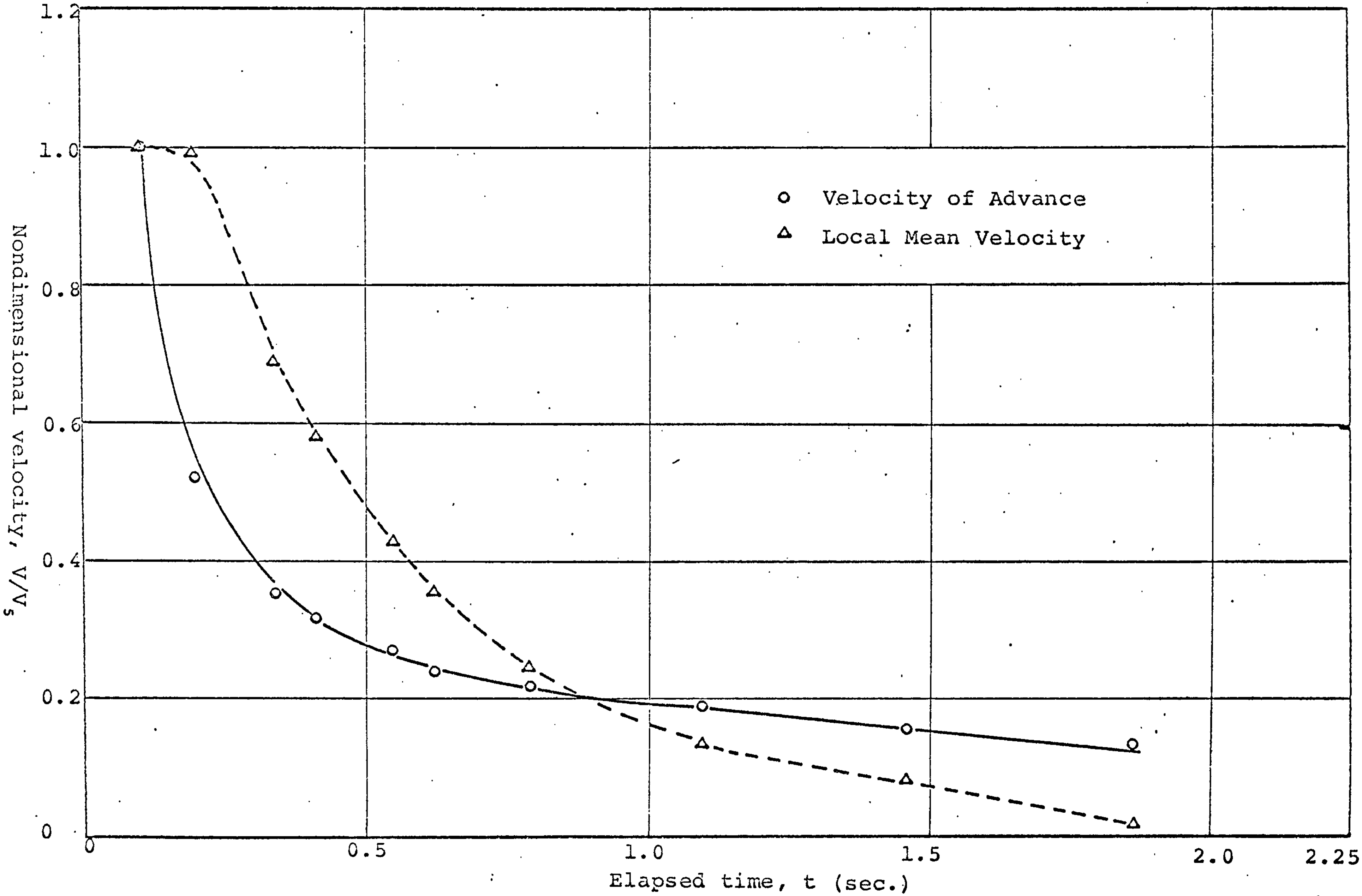

FIGURE 5. ADVANCE VELOCITY OF A RING VERSUS ELAPSED TIME (1)

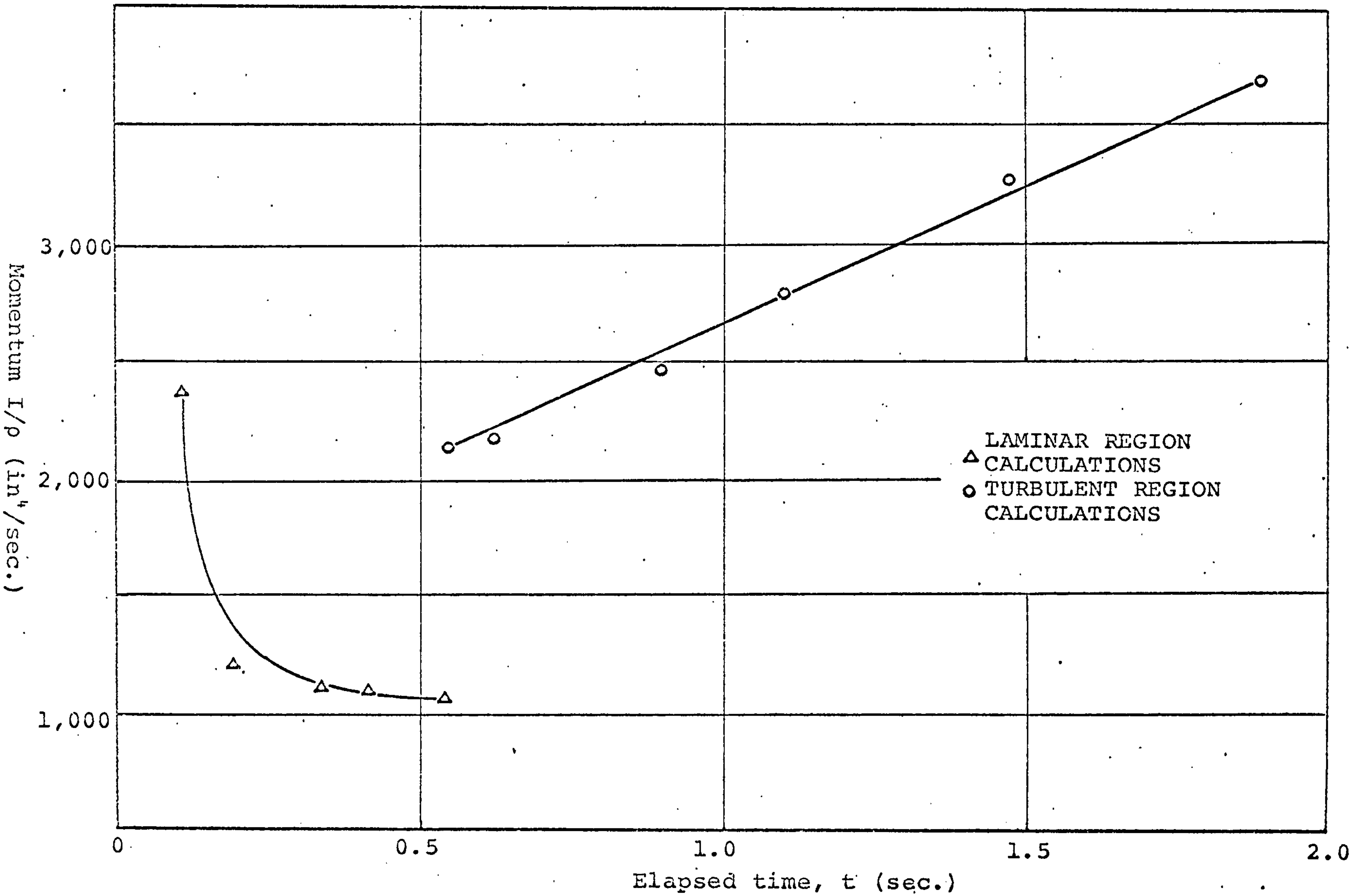

FIGURE 6. LINEAR MOMENTUM I/ρ VERSUS ELAPSED TIME, t

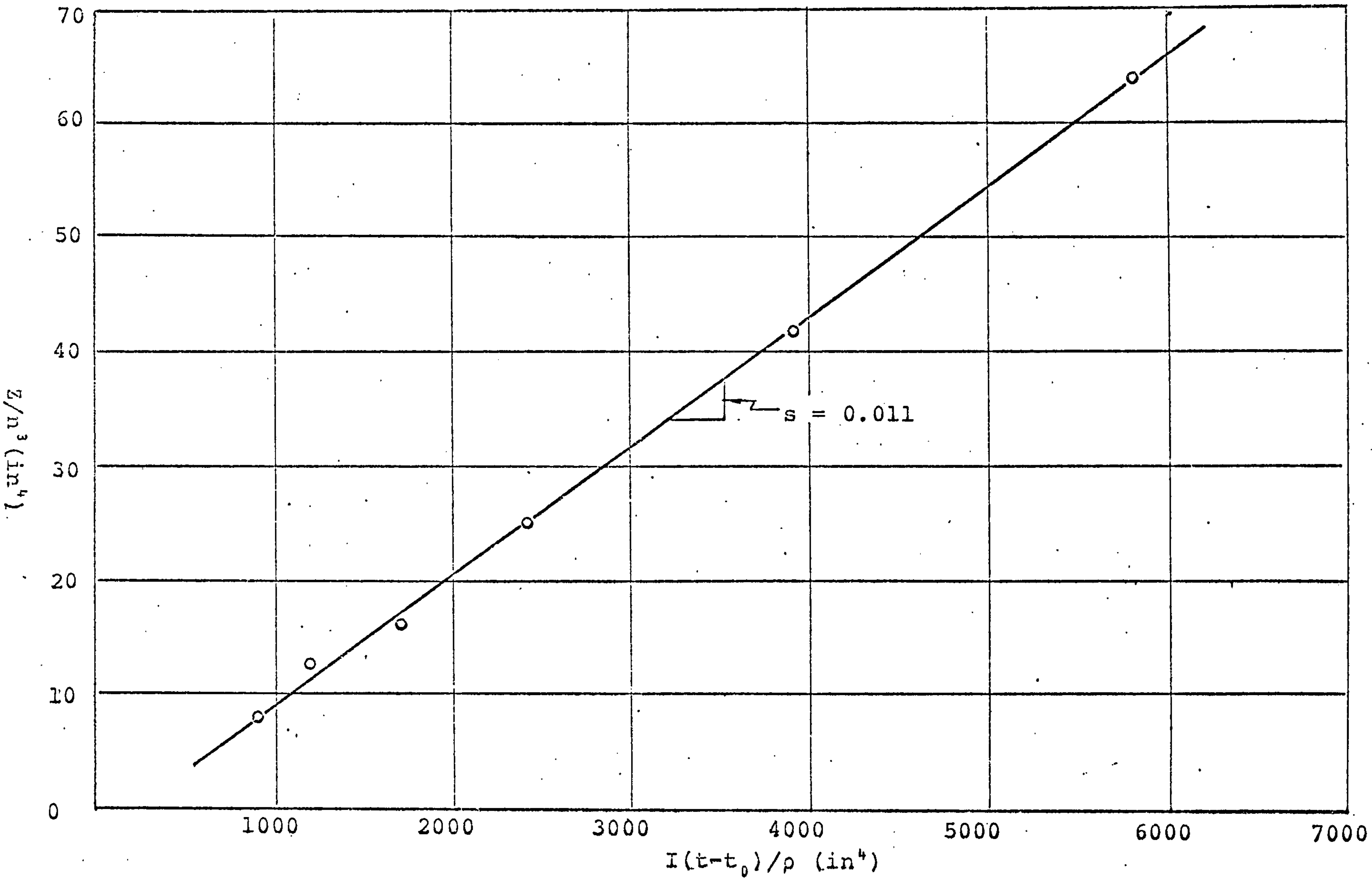

FIGURE 7. PLOT OF CALCULATED VALUES OF IMPULSE FROM EQUATION (29)